coatings

MDPI

Article

Stiffness Degradation of Expansive Soil Stabilized with Construction and Demolition Waste Under Wetting–Drying Cycles

Haodong Xu and Chao Huang *

School of Civil Engineering, Central South University, Changsha 410075, China
* Correspondence: huangchao-22@csu.edu.cn

Abstract

To address the challenge of long-term stiffness retention of subgrades in humid–hot climates, this study evaluates expansive soil stabilized with construction and demolition waste (CDW), focusing on the resilient modulus (M_r) under coupled stress states and wetting–drying histories. Basic physical and swelling tests identified an optimal CDW incorporation of about 40%, which was then used to prepare specimens subjected to controlled. Wetting–drying cycles (0, 1, 3, 6, 10) and multistage cyclic triaxial loading across confining and deviatoric stress combinations. M_r increased monotonically with both stresses, with stronger confinement hardening at higher deviatoric levels; with cycling, M_r exhibited a rapid then gradual degradation, and for most stress combinations, the ten-cycle loss was 20%–30%, slightly mitigated by higher confinement. Grey relational analysis ranked influence as follows: the number of wetting–drying cycles > deviatoric stress > confining pressure. A Lytton model, based on a modified prediction method, accurately predicted M_r across conditions ($R^2 \approx 0.95$–0.98). These results integrate stress dependence with environmental degradation, offering guidance on material selection (approximately 40% incorporation), construction (adequate compaction), and maintenance (priority control of early moisture fluctuations), and provide theoretical support for durable expansive soil subgrades in humid–hot regions.

Keywords: subgrade; construction and demolition waste; stabilized expansive soil; wetting–drying cycles; resilient modulus

Academic Editor: Andrea Simone

Received: 8 September 2025
Revised: 26 September 2025
Accepted: 29 September 2025
Published: 3 October 2025

Citation: Xu, H.; Huang, C. Stiffness Degradation of Expansive Soil Stabilized with Construction and Demolition Waste Under Wetting–Drying Cycles. *Coatings* **2025**, *15*, 1154. https://doi.org/10.3390/coatings15101154

1. Introduction

The resilient modulus (M_r) is a primary indicator of subgrade stiffness and has long been central in pavement engineering [1,2]. M_r directly informs fatigue cracking predictions and structural layer thickness design [3], and insufficient M_r is a key contributor to rutting distress [4]. In the humid and hot regions of southern China, for example Hunan and Jiangxi, frequent rainfall and high climatic variability threaten subgrade stability, and accumulating evidence shows that soil type and environmental exposure exert non-negligible influences on stiffness performance [5]. From the perspectives of design, construction, and maintenance, elucidating how subgrade stiffness evolves under wetting and drying cycles is therefore of clear engineering significance.

Expansive soil is widely distributed across these regions [6,7] and is often used as subgrade fill when conventional aggregates are scarce [8]. Yet its fissured fabric with swelling and shrinkage, which is characterized by multiple crack networks, water-induced

expansion, and drying contraction, renders subgrades vulnerable to stiffness deterioration under repeated traffic loading [9,10], thereby posing substantial risks to highway performance [11]. Chemical stabilization using cement or quicklime is common practice to ensure service stability and durability [12,13]; however, the efficacy of such treatments is time-dependent and may impose environmental burdens.

Meanwhile, rapid urbanization has sharply increased construction and demolition waste (CDW), and the challenges of CDW disposal and reuse are constraining sustainable urban development [14]. Processing CDW into recycled aggregates through crushing, screening, and impurity removal enables road engineering applications that consume large volumes of waste and also mitigate the impacts associated with quarrying and extensive earthwork, which in turn reduces costs, energy use, and emissions [15–19]. Recent studies further indicate that incorporating CDW can improve problematic soils from hydromechanical and mechanical perspectives [20,21], thereby providing systematic evidence for engineering application [22].

Against this backdrop, this study investigates expansive soil from a highway reconstruction project in Hunan that is stabilized with locally sourced CDW. Distinct from prior efforts that considered swelling reduction or strength gain in isolation, the present work addresses the lack of an integrated framework that couples stress dependence with environmental degradation for CDW-stabilized expansive soils. A laboratory program was designed to identify the optimal replacement range using swelling and hydromechanical indices, and to evaluate the combined influence of stress state and wetting and drying cycles on the resilient modulus by means of multistage cyclic triaxial tests. Grey relational analysis was then employed to rank factor sensitivity, thereby establishing a stress and environmental degradation framework that advances both mechanistic understanding and engineering.

2. Materials and Methods

2.1. Materials

Untreated soil was sampled from a first-class highway reconstruction project in south central China. Basic physical properties and swelling characteristics were determined in accordance with the Test Methods of Soils for Highway Engineering (JTG 3430–2020) [23] and are summarized in Table 1. The soil is classified as weakly expansive and, in its native state, is unsuitable for direct subgrade filling.

Table 1. Basic physical properties of expansive soil.

Specific Gravity	Liquid Limit (%)	Plastic Limit (%)	Maximum Dry Density (g/cm^3)	Optimum Moisture Content (%)	Free Swell Index (%)	Clay Content (%)	Silt Content (%)	Sand Content (%)
2.7	42.3	24.8	1.68	14.8	46.7	25.4	39.8	34.8

The CDW was obtained from residential demolitions along the project corridor, Table 2 shows the basic physical properties of CDW. The material, composed primarily of concrete fragments, bricks, and mortar, was crushed, sieved, and cleaned to meet specimen size and triaxial apparatus requirements, while removing visible contaminants (for example, gypsum board and coated debris) to reduce the risk of excess chlorides, sulfates, and heavy metals. X-ray diffraction (Bruker D8 Advance, Billerica, MA, USA) of the processed CDW (Figure 1) identified quartz, calcite, illite, and potassium feldspar as the dominant crystalline phases, consistent with masonry and concrete debris.

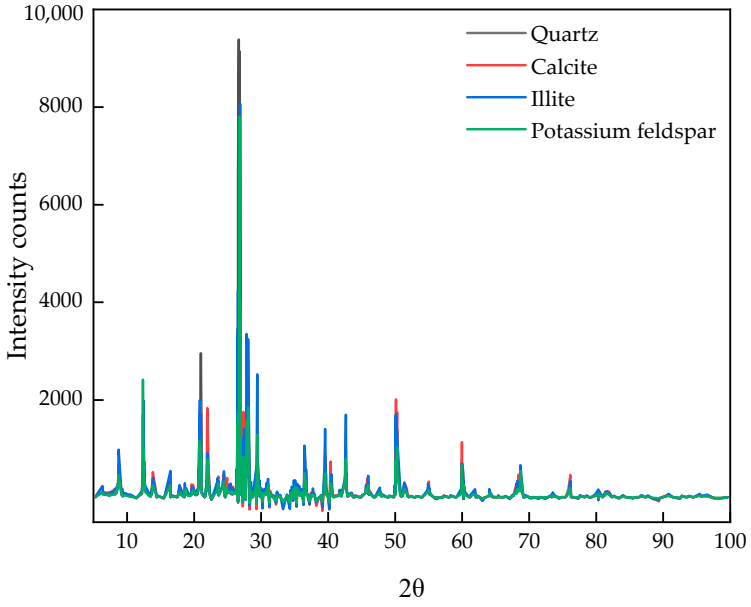

Figure 1. Results of compositional analysis tests.

Leaching tests on the CDW (Figure 2) quantified Cd, Pb, and As. The maximum concentrations (Cd 0.09 μg·L^{-1}; Pb 2.8 μg·L^{-1}; As 17 μg·L^{-1}) were below the Class I groundwater thresholds specified in GB/T 14848–2017 (Cd 1 μg·L^{-1}; Pb 10 μg·L^{-1}; As 50 μg·L^{-1}) [24]. Where site conditions suggest possible exceedances, mitigation can include selective source control (excluding gypsum, painted or coated debris, and treated timber), enhanced pre-treatment such as washing and fine removal, and blending with binders or additives that immobilize harmful ions.

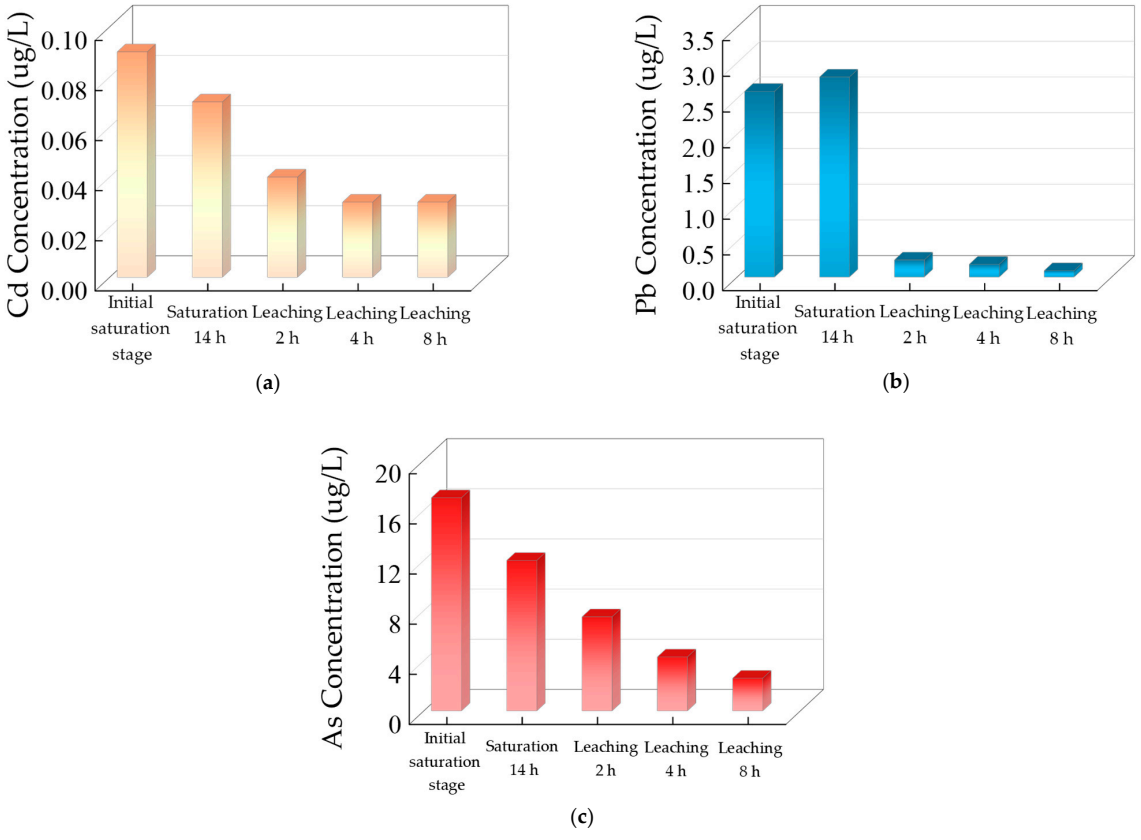

Figure 2. Leaching test results: (**a**) Cd; (**b**) Pb; (**c**) As.

To minimize size effects and ensure gradation repeatability, the maximum particle size was limited to ≤20 mm, i.e., less than one-fifth of the specimen diameter (150 mm) [25].

In addition, a 3D laser scanning test was performed on 200 randomly selected CDW particles to obtain particle shape parameters, Figure 3 shows the experimental apparatus, and the results are shown in Figure 4. The particle shape distribution was relatively concentrated, with most particle sphericity values ranging from 0.67 to 1. The majority of particles exhibited bulky shapes, while a smaller proportion were disc-shaped, and elongated or flake particles were rare. Due to resource limitations, the influence of particle shape on the test results was not considered in this study but will be investigated in future research.

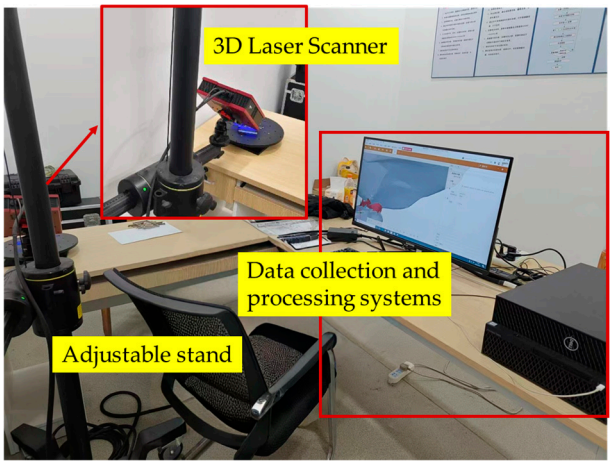

Figure 3. Apparatus for 3D laser scanning test.

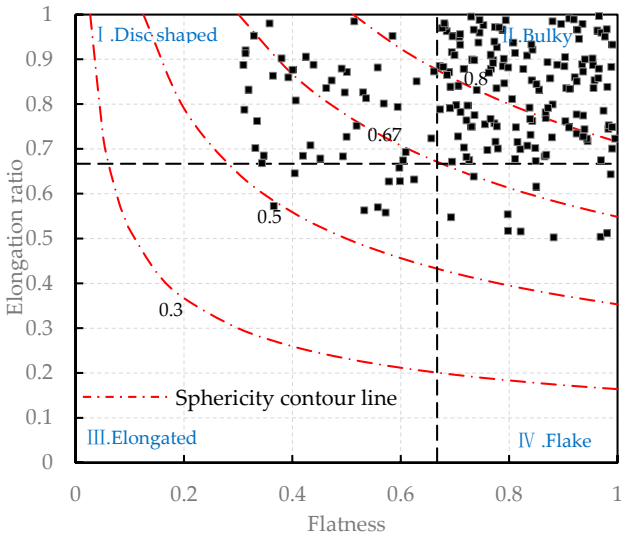

Figure 4. Classification results of CDW particle shapes.

Table 2. Basic physical properties of CDW.

Natural Moisture Content (%)	Specific Gravity	Coefficient of Uniformity	Coefficient of Curvature	Fine Content (%)	Sand Content (%)	Gravel Content (<20 mm) (%)
13.5	2.26	2.45	0.79	8.5	31.8	59.7

2.2. Determination of the Optimal Gradation of the Stabilized Soil

2.2.1. Influence of CDW Content on Swelling Behavior

Mixtures with CDW replacement levels of 0%, 20%, 30%, 40%, and 50% were prepared, and the gradation curves of these mixtures are shown in Figure 5. The free swell ratio, unconfined swell ratio, confined (loaded) swell ratio, and swelling pressure were measured (Figure 6). With 50% CDW, the free swell ratio decreased from 45.7% to 18.79%, the unconfined swell ratio decreased from 11.20% to 8.27%, the loaded swell ratio decreased from 1.75% to 0.437%, and the swelling pressure decreased from 88.9 kPa to 26.00 kPa. These results indicate a monotonic suppression of swelling with increasing CDW content. Notably, for contents between 30% and 50%, the free swell ratio remained below 40%, which satisfies the deformation control requirement for subgrade fill in JTG/T 3610–2019 [24]. The reduction mechanism has two main aspects: first, partial replacement of clay-sized fractions lowers mineral specific surface area and the thickness of the adsorbed water film, which weakens double-layer interactions; second, the coarse particle skeleton provides interlocking and frictional restraint, so the loaded swelling shows higher sensitivity to CDW content [25].

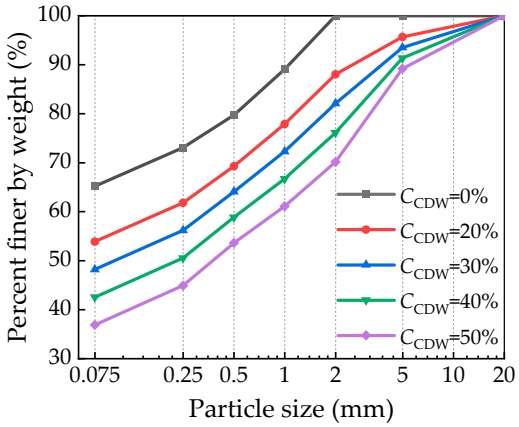

Figure 5. Gradation curves of mixtures with different CDW replacement levels.

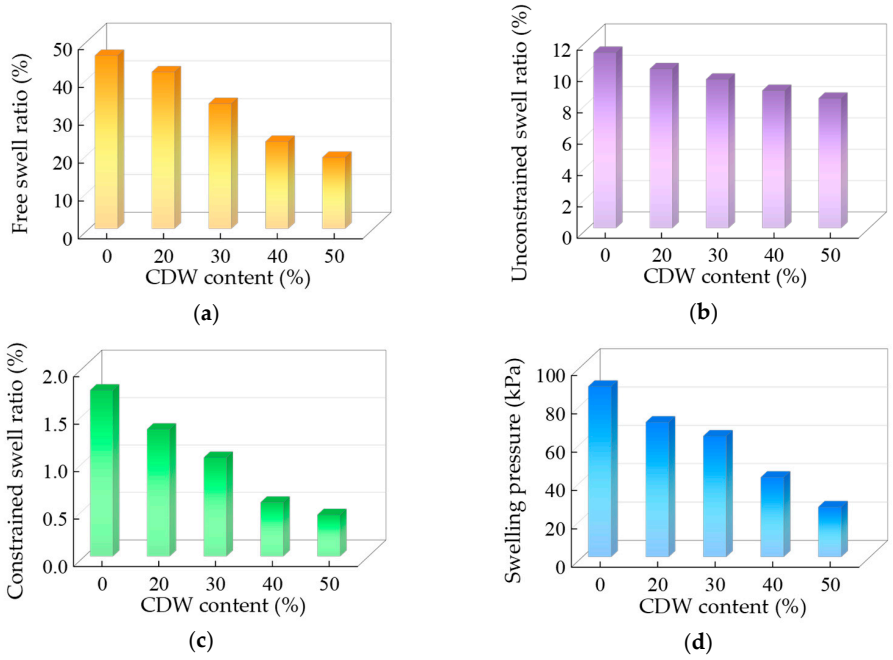

Figure 6. Swelling characteristics of CDW-stabilized expansive soil at different incorporation ratios: (**a**) free swell index; (**b**) unconstrained swell ratio; (**c**) constrained swell ratio; (**d**) swelling pressure.

2.2.2. Influence of CDW Content on Physical Properties

Atterberg limits, heavy compaction characteristics, and four-day soaked CBR were determined in accordance with JTG 3430–2020 (Figure 7) [23].

i. Atterberg limits showed an overall decline. From 0% to 50% CDW, the liquid limit decreased from 42.3% to 23.1%, the plastic limit decreased from 24.8% to 17.4%, and the plasticity index decreased from 17.5 to 5.7, indicating reduced plasticity and moisture sensitivity.

ii. Compaction characteristics first increased and then decreased. The maximum dry density ranged from 1.68 to 1.77 g·cm^{-3} and reached a peak value of 1.77 g·cm^{-3} at 40% CDW, which is about 5.4% higher than that of untreated soil. The optimum moisture content decreased from 14.8% to 8.8%, i.e., a reduction of 40.5%. This pattern suggests that a moderate content promotes a dense coarse skeleton, whereas excessive content leaves insufficient fines to fill voids, so the density declines.

iii. Bearing capacity improved markedly and exhibited an optimum. Soaked CBR increased with content and then slightly decreased, reaching 25.1% at 40% CDW, which is about 5.23 times that of untreated soil, and then slightly falling to 23.4% at 50% CDW. The slight decrease can be inferred from existing studies to result from fine deficiency and localized particle breakage [26]. Considering both swelling suppression and structural capacity, 40% CDW was adopted as the optimum content for subsequent tests.

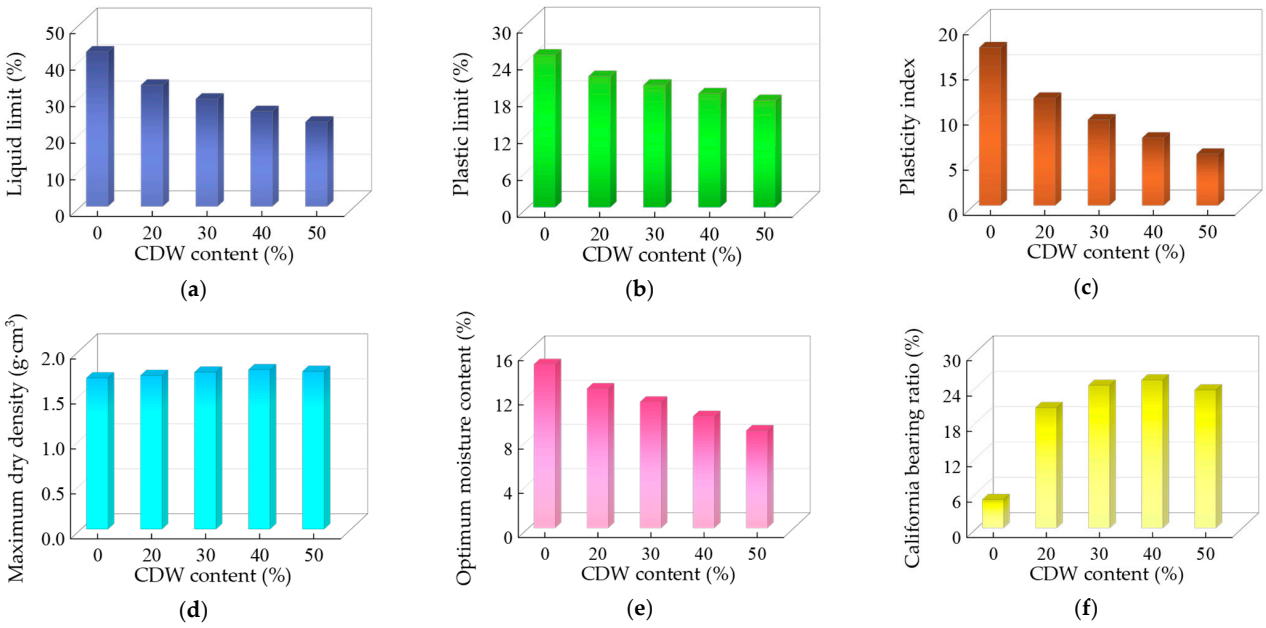

Figure 7. Physical properties of CDW-stabilized expansive soil at different incorporation ratios: (**a**) liquid limit; (**b**) plastic limit; (**c**) plasticity index; (**d**) maximum dry density; (**e**) optimum moisture content; (**f**) CBR.

2.3. Wetting and Drying Protocol and Resilient Modulus Testing

Based on Section 2.2, all subsequent tests used 40% CDW. Cylindrical specimens with a diameter of 150 mm and a height of 300 mm were prepared via static compaction to a target degree of compaction of 95% at the optimum moisture content corresponding to the 40% mix. Layered compaction and checks of mass and volume were employed to ensure uniformity, and deviations in the achieved compaction and moisture content were controlled within ± 1%. After forming, specimens were sealed to allow internal moisture to equilibrate.

The numbers of wetting and drying cycles were set to N_{dw} = 0, 1, 3, 6, and 10. This choice was made with reference to previous studies, which consistently report that the mechanical properties of geomaterials tend to stabilize after about five cycles, and that ten cycles are widely adopted in laboratory practice as a reasonable and conservative approximation of long-term degradation trends [4,5,27–29]. Each cycle included three steps.

i. Humidification: the specimen was sealed in a controlled humidity environment until its mass stabilized, which required about 48 h.
ii. Air drying: natural drying at 25 °C until the mass returned to the value measured before humidification.
iii. Equalization: sealing for 24 h to equilibrate the internal moisture state.

After the prescribed cycles, resilient modulus testing was conducted.

The resilient modulus (M_r) was obtained using a Dynatriax 100/14 automated cyclic triaxial system (Figure 8). A half sine pulse was applied at a frequency of 1 Hz with a load duration of 0.2 s and a rest period of 0.8 s. Confining and deviatoric stress sequences are shown in Table 3. In accordance with JTG 3430–2020, the stable response from cycle 96 to cycle 100 in each stress state was used to compute the recoverable axial strain εR, and M_r was then calculated by using Equation (1).

$$M_r = \frac{\sigma_d}{\varepsilon_r}, \quad (1)$$

where M_r is the resilient modulus, σ_d is the peak cyclic deviator stress, and ε_r is the peak resilient axial strain.

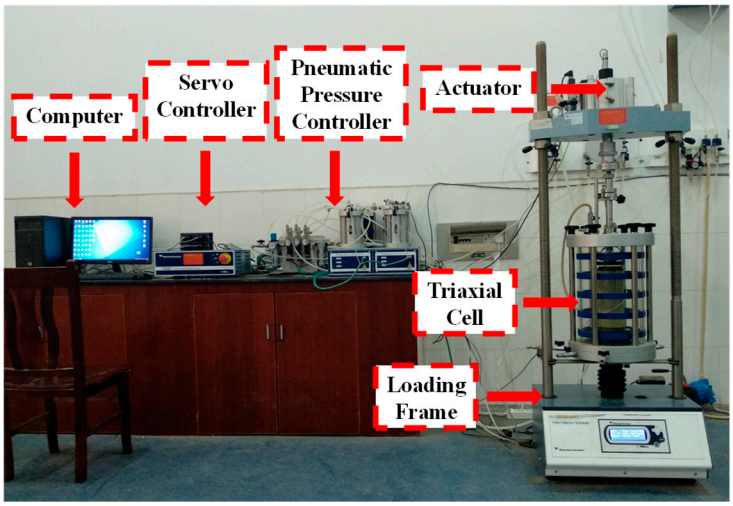

Figure 8. Schematic of triaxial apparatus.

Table 3. Resilient modulus loading sequence recommended by JTG 3430–2020.

Seq. No.	Confining Pressure, σ_3 (kPa)	Contact Stress, $0.2\sigma_3$ (kPa)	Cyclic Deviator Stress, σ_d (kPa)	Principal Stress Ratio, $r = \sigma_1/\sigma_3$	No. of Cycles
0 (Preloading)	30	6	60	3	1000
1	15	3	8	1.5	100
2	30	6	15	1.5	100
3	45	9	23	1.5	100
4	60	12	30	1.5	100
5	80	16	40	1.5	100

Table 3. *Cont.*

Seq. No.	Confining Pressure, σ_3 (kPa)	Contact Stress, $0.2\sigma_3$ (kPa)	Cyclic Deviator Stress, σ_d (kPa)	Principal Stress Ratio, $r = \sigma_1/\sigma_3$	No. of Cycles
6	15	3	15	2	100
7	30	6	30	2	100
8	45	9	45	2	100
9	60	12	60	2	100
10	80	16	80	2	100
11	15	3	30	3	100
12	30	6	60	3	100
13	45	9	90	3	100
14	60	12	120	3	100
15	80	16	160	3	100

3. Results and Discussion

3.1. Effect of Stress State on Resilient Modulus

The resilient modulus (M_r) shows clear dependence on the stress state (Figure 9). Using the case without wetting and drying cycles (N_{dw} = 0) as an example, when the stress ratio $r = \sigma_d/\sigma_3$ equals 0.5, increasing the confining pressure from 15 kPa to 80 kPa raises M_r from 49.95 MPa to 126.54 MPa, an increase of about 153 percent. At r = 1.0, the corresponding M_r increases from 54.87 MPa to 152.50 MPa, an increase of about 178 percent. At r = 2.0, M_r increases from 60.23 MPa to 180.74 MPa, an increase of about 200 percent. This monotonic rise persists at all levels of N_{dw}. Only minor fluctuations appear at low confining pressure and intermediate cycle counts, which do not alter the overall trend. Across stress ratios, confining pressure not only elevates M_r but also exhibits a stronger hardening effect at higher deviatoric stress, indicating a coupling between confining pressure sensitivity and the level of deviatoric stress [30].

At fixed confining pressure, M_r is also sensitive to deviatoric stress. At σ_3 = 45 kPa, when σ_d increases from 23 kPa to 45 kPa and then to 90 kPa, M_r equals 86.69, 98.96, and 119.77 MPa. Relative to the lower deviatoric stress case, M_r increases by about 14 percent and then by about 38 percent. At σ_3 = 80 kPa, M_r equals 126.54, 152.50, and 180.74 MPa for the same sequence of σ_d, which corresponds to increases of about 21 percent and about 43 percent. A larger deviatoric stress promotes greater tangential contact stiffness and a larger effective load-bearing area; interlocking and resistance to rolling become stronger [31], which reduces the recoverable strain per unit deviatoric stress and thus raises M_r. The joint features of positive correlation with confining pressure and with deviatoric stress, together with their coupling, agree with stress-dependent empirical forms widely used for unbound layers. In the formulations associated with Hicks and Monismith and with Uzan, M_r increases as a power of bulk or effective confining stress and shows positive sensitivity to the level of shear stress [32].

3.2. Effect of Environmental History on Resilient Modulus

In a given stress state, M_r declines with an increasing number of wetting and drying cycles (Figure 10). The decline is faster at the beginning and becomes slower later. Under a high-stress combination (σ_3 = 80 kPa, σ_d = 160 kPa), when N_{dw} increases from 0 to 10, M_r decreases from 180.74 MPa to 151.16, 141.00, 135.29, and 129.06 MPa. The overall reduction is about 29 percent. Under a low-stress combination (σ_3 = 15 kPa, σ_d = 8 kPa), M_r decreases from 49.95 MPa to 36.25 MPa as N_{dw} increases from 0 to 10, a reduction of about 27 percent. For most stress combinations, the total reduction falls between 20 percent and 30 percent,

with the initial drop from N_{dw} = 0 to N_{dw} = 1 being the most prominent. For example, at σ_3 = 80 kPa and σ_d = 40 kPa, M_r decreases from 126.54 MPa to 107.35 MPa, a reduction of about 15 percent. From N_{dw} = 3 to N_{dw} = 10, it decreases slowly from 95.98 MPa to 89.64 MPa. In general, combinations with higher confining pressure show a slightly smaller reduction, which indicates that confining pressure can delay the stiffness loss induced by wetting and drying.

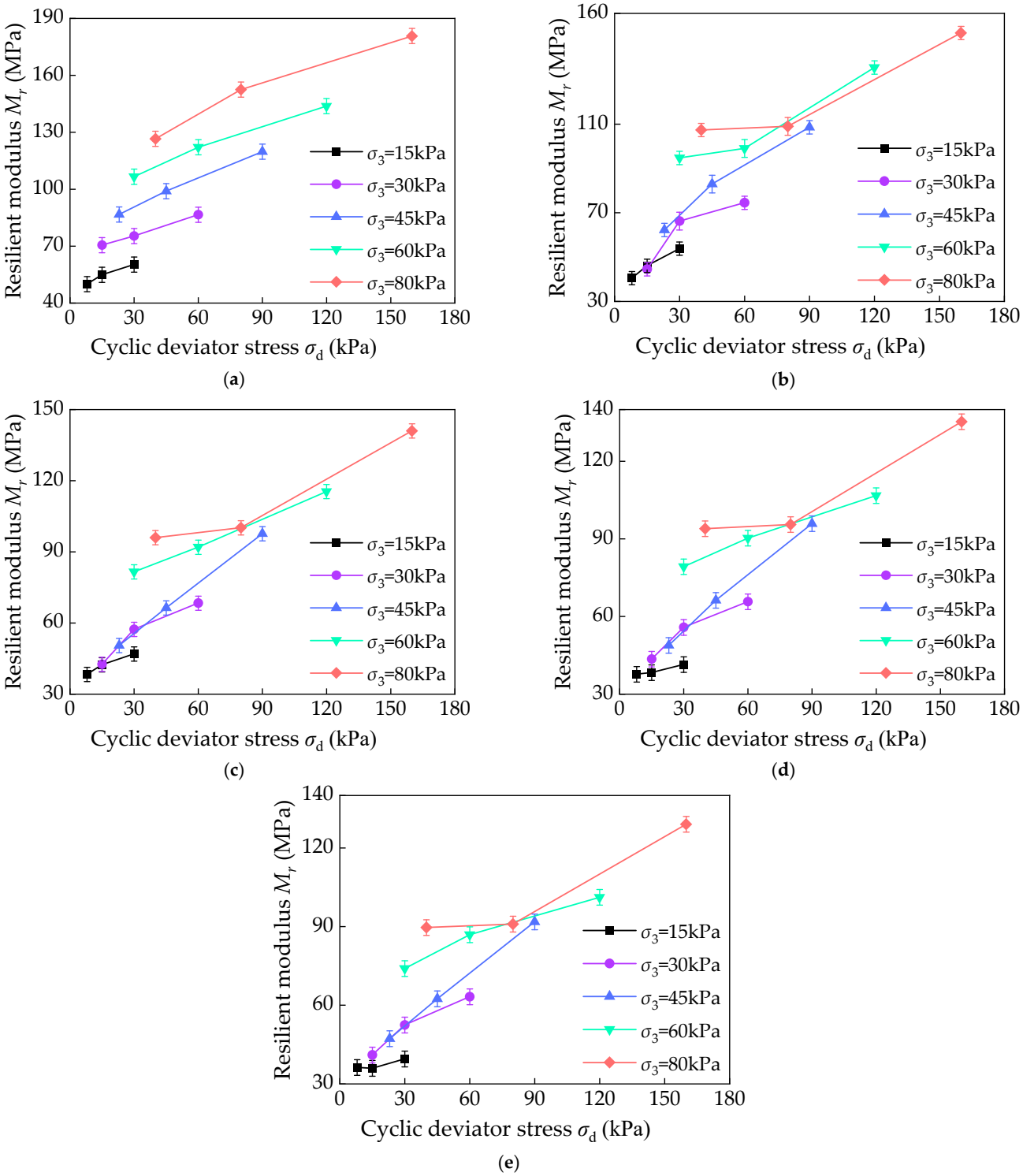

Figure 9. Resilient modulus of each specimen group under different stress states: (**a**) N_{dw} = 0; (**b**) N_{dw} = 1; (**c**) N_{dw} = 3; (**d**) N_{dw} = 6; (**e**) N_{dw} = 10.

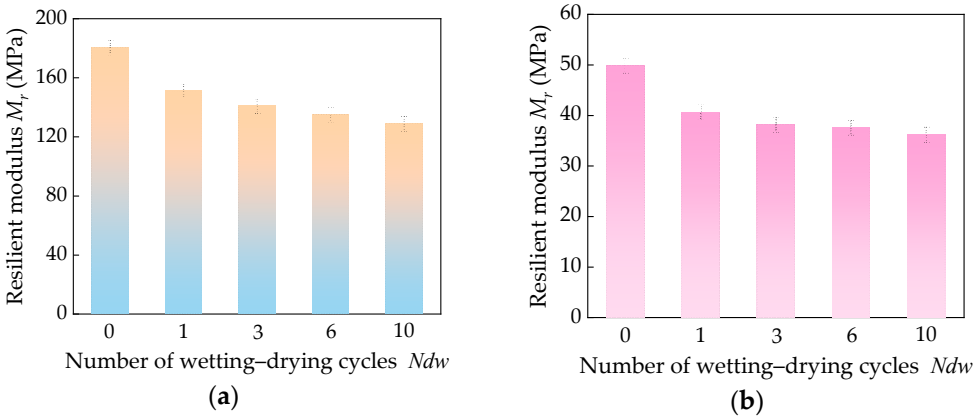

Figure 10. Resilient modulus of each specimen group under different wetting and drying cycles: (**a**) σ_3 = 80 kPa, σ_d = 160 kPa; (**b**) σ_3 = 15 kPa, σ_d = 8 kPa.

Mechanistically, the influence of wetting and drying can be plausibly interpreted through three pathways, as supported by previous studies on expansive soils and similar geomaterials. First, repeated humidification and drying reduce matric suction and alter the relation between suction and water content, which lowers the effective stiffness [33,34]. Second, swelling and shrinkage produce microcracks and reconfigured pores that disrupt the continuity of force chains and lower effective contact stiffness. Under higher confining pressure, the force chains become more continuous and are more readily compacted, which leads to a slower rate of degradation [35,36]. Third, edge rounding and localized microcrushing reduce interlocking and frictional restraint and thereby increase the recoverable strain [37,38]. Prior studies have shown that M_r is highly sensitive to moisture and suction, that wetting and drying cycles cause cumulative degradation, and that a suitable level of confining pressure can delay this process [39]. The present data reproduce these behaviors across different confining pressures, which supports the development of a degradation model that incorporates both the stress state and the environmental history.

In addition, Abbey et al. investigated expansive soils stabilized with sustainable cementitious waste materials for use as subgrade fill. Their results showed that after ten wetting–drying cycles, M_r decreased by approximately 50% [40]. This comparison indicates that using CDW as a stabilizer offers a relative advantage, as the modulus reduction observed is less severe, thereby supporting the suitability of CDW-stabilized expansive soil for subgrade applications.

3.3. Sensitivity of Dynamic Resilient Modulus to Influencing Factors

To compare how confining pressure, deviatoric stress, and the number of wetting and drying cycles affect the M_r of CDW-stabilized expansive soil, a grey relational analysis is conducted to rank factor importance [41]. The goal is to identify which factor primarily weakens stiffness in humid and hot regions and to provide guidance for durable subgrade design.

The procedure follows four steps. First, the M_r measured under each working condition is taken as the reference sequence $X_0 = \{x_0(k), k = 1, 2, \ldots n\}$. Each influencing factor—confining pressure, deviatoric stress, and the number of wetting and drying cycles—is taken as a comparison sequence $X_i = \{x_i(k), k = 1, 2, \ldots n\}$.

$$\widetilde{X_i}(k) = \frac{x_i(k)}{x_i(1)}; \widetilde{X_0}(k) = \frac{x_0(k)}{x_0(1)}, \tag{2}$$

where $\widetilde{X_i}(k)$ is the comparison sequence normalized to a dimensionless form by initial value processing, $\widetilde{X_0}(k)$ is the reference sequence normalized to a dimensionless form

by standardization, k is the index of the working condition, and i is the index of the influencing factor.

Second, we apply Equation (3) to obtain the proximity measure between each factor's initial value-normalized sequence and the corresponding test results:

$$\Delta_i(k) = \left|\widetilde{X_i}(k) - \widetilde{X_0}(k)\right|, \tag{3}$$

Third, we apply Equation (4) to obtain the grey relational coefficient:

$$\xi_i(k) = \frac{\Delta_{\min} + \rho\Delta_{\max}}{\Delta_i(k) + \rho\Delta_{\max}}, \tag{4}$$

where $\xi_i\ (k)$ is the grey relational coefficient between factor i and the test result under working condition k; $\Delta_{\min}$ and $\Delta_{\max}$ are, respectively, the minimum and the maximum of all proximity values obtained in Equation (3); ρ is the distinguishing coefficient, taken as between 0.5 and 0.6 (here a value of 0.6 is adopted to balance resolution and numerical stability) [41].

Finally, we apply Equation (5) to obtain the grey relational degree for each factor relative to the test results:

$$\gamma_i = \frac{1}{n}\sum_{k=1}^{n} \xi_i(k), \tag{5}$$

where γ_i denotes the grey relational degree of factor i, and n is the total number of working conditions.

Applying this procedure yields the following ranking of influence: the number of wetting and drying cycles (γ = 0.931) greater than deviatoric stress (γ = 0.907) greater than confining pressure (γ = 0.885). This resembles what Figure 11 shows. Thus, environmental history exerts the strongest weakening effect on the resilient response, while the stress state also plays an important and positive role. The difference between deviatoric stress and confining pressure is small in a statistical sense, indicating comparable contributions to stiffness enhancement when moisture history is fixed.

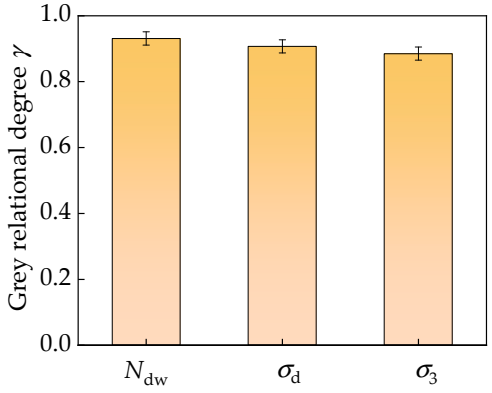

Figure 11. Grey relational degree of each factor.

These results suggest that models and engineering design for CDW-stabilized subgrades in humid and hot regions should explicitly account for the cumulative degradation caused by wetting and drying cycles and the combined effect of confining pressure and deviatoric stress. Doing so will help maintain stiffness and stability during service.

3.4. Model Analysis

Based on the resilient modulus test results and the outcomes of the grey relational analysis, the Lytton model recommended by JTG 3430–2020 [23] was used for fitting. The

fitted model enables the prediction of the resilient modulus of CDW-stabilized expansive soil under varying numbers of wetting–drying cycles, deviatoric stresses, and confining pressures. The model parameters are presented in Table 4, and the robustness of the model is validated in Figure 12.

Table 4. Model parameters.

N_{dw}	k_1	k_2	k_3	R^2	RMSE	Correlation
0	0.66	0.58	0.34	0.98	3.12	Excellent
1	0.53	0.50	0.65	0.95	4.98	Excellent
3	0.46	0.49	0.76	0.96	4.22	Excellent
6	0.45	0.52	0.64	0.96	4.22	Excellent
10	0.43	0.52	0.65	0.95	4.98	Excellent

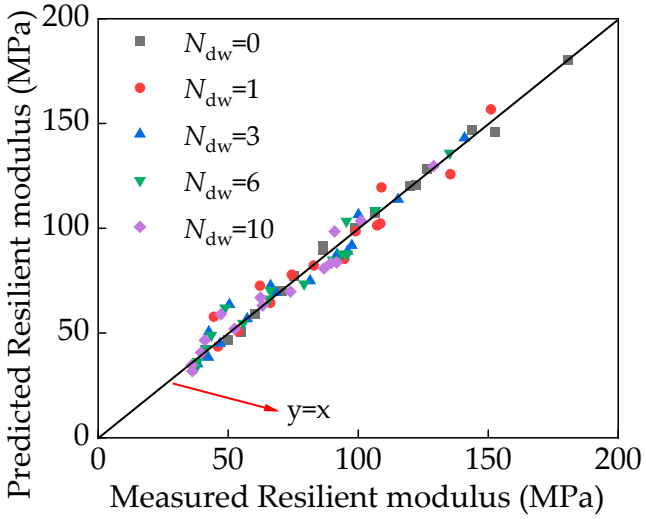

Figure 12. Robustness verification.

The Lytton model is given by the following:

$$M_r = k_1 P_a \left(\frac{\theta}{P_a}\right)^{k_2} \left(\frac{\tau_{oct}}{P_a} + 1\right)^{k_3}, \quad (6)$$

where M_r is the resilient modulus; θ is the bulk stress; τ_{oct} is the octahedral shear stress; k_1, k_2, and k_3 are regression coefficients, with $k_1 \geq 0$, $k_2 \geq 0$, and $k_3 \leq 0$; and P_a is the reference atmospheric pressure, taken as 100 kPa. The expressions for θ and τ_{oct} are given in Equations (7) and (8).

$$\theta = 3\sigma_3 + \sigma d, \quad (7)$$

$$\tau_{oct} = \sqrt{(\sigma_1 - \sigma_2)^2 + (\sigma_1 - \sigma_3)^2 + (\sigma_2 - \sigma_3)^2}/3 = \left(\sqrt{2}/3\right)\sigma_d, \quad (8)$$

It can be observed that the experimental measurements and the model predictions presented in this section exhibit strong correlation. To further validate the robustness of the model, a scatter plot was constructed based on the measured and predicted resilient modulus values (Figure 12). In the figure, the measured resilient modulus is plotted on the horizontal axis and the predicted values on the vertical axis, with the scatter distribution providing a direct visualization of the model's predictive performance. As shown in Figure 12, most data points are closely clustered around the line y = x, indicating that the model provides a good fit to the experimental data. In summary, the fitting analysis and robustness verification demonstrate that the resilient modulus prediction model adopted

in this study not only exhibits strong representativeness but also achieves accuracy and stability sufficient for general engineering applications.

4. Conclusions

In summary, this study systematically evaluated the mechanical performance of expansive soil stabilized with construction and demolition waste under combined stress and environmental actions. Through swelling tests, hydromechanical characterization, multistage cyclic triaxial testing, and model analysis, the effects of CDW content, stress state, and wetting–drying cycles on stiffness evolution were clarified. The results not only identified the optimal replacement range but also established a stress and environmental degradation framework and a predictive model that provide both mechanistic insight and practical guidance for the design and long-term maintenance of CDW-stabilized subgrades.

(1) An optimal CDW content of about 40% was identified, effectively reducing swelling potential while improving compaction and bearing capacity. This mix proportion provides a practical guideline for material selection in subgrade construction.
(2) The resilient modulus exhibited typical stress dependence: it increased monotonically with confining pressure and deviatoric stress, with stronger hardening observed under higher deviatoric stress. These findings confirm that appropriate stress conditions can be used to enhance the stiffness performance of stabilized subgrades.
(3) Wetting–drying cycles induced stiffness degradation, with a rapid initial drop followed by a gradual decline. Higher confining pressure delayed this deterioration, suggesting that adequate overburden or compaction control in the field could mitigate stiffness loss.
(4) Grey relational analysis identified the number of wetting–drying cycles as the dominant factor, followed by deviatoric stress and confining pressure. This ranking underscores the importance of moisture management over purely mechanical considerations.
(5) By incorporating the experimental results into the Lytton model, a modified prediction framework was established. The fitted parameters achieved a high degree of accuracy ($R^2 \geq 0.95$) across all conditions, and robustness verification demonstrated strong agreement between predicted and measured resilient modulus values. This indicates that the model is reliable and suitable for engineering applications.
(6) For long-term pavement service, CDW-stabilized subgrades should be constructed at the optimal content with strict control of moisture and compaction. Maintenance strategies should focus on early cycle moisture fluctuations, which exert the greatest impact on stiffness, and apply predictive models that couple stress dependence with cyclic degradation for reliable service life evaluation.

Despite the valuable findings obtained in this study, certain limitations remained. Due to equipment and funding constraints, direct microstructural observations such as SEM and micro-CT were not conducted. As a result, the mechanistic explanations of pore reconfiguration, microcrack development, and particle breakage were still partly qualitative and literature-based, lacking comprehensive direct evidence. Future work will incorporate chemical and microstructural characterization to verify these mechanisms and will extend environmental risk assessments to ensure the long-term durability and safety of CDW-stabilized soils. In addition, the scope of investigation will be broadened from wetting–drying cycles to other environmental actions such as freeze–thaw and chemical attack, thereby establishing a more complete framework for evaluating the service performance of CDW-stabilized expansive soils.

Author Contributions: H.X.: investigation, data curation, writing—original draft. C.H.: conceptualization, methodology, software, writing—original draft. All authors have read and agreed to the published version of the manuscript.

Funding: This research was supported by the Research and Innovation Project for Graduate Students at Central South University (Grant No. 1053320232288) and the Henan Provincial Key Science and Technology Research Project (No. 252102240019).

Institutional Review Board Statement: Not applicable.

Informed Consent Statement: Not applicable.

Data Availability Statement: The original contributions presented in this study are included in the. article.: Further inquiries can be directed to the corresponding author.

Conflicts of Interest: The authors declare no conflicts of interest.

Abbreviations

The following abbreviations are used in this manuscript:

M_r	Resilient Modulus
CDW	Construction and Demolition Waste
CBR	California Bearing Ratio
N_{dw}	Number of Wetting and Drying Cycles
σ_d	Peak Cyclic Deviator Stress
ε_r	Peak Resilient Axial Strain
σ_3	Confining pressure
r	Principal Stress Ratio
γ	Grey Relational Degree
$\widetilde{X_i}(k)$	The Comparison Sequence Normalized to a Dimensionless Form by Initial Value Processing
$\widetilde{X_0}(k)$	The Reference Sequence Normalized to a Dimensionless Form by Standardization
k	Index of the Working Condition
i	Index of the Influencing Factor
$\xi_i\,(k)$	Grey Relational Coefficient
Δ_{min}	Minimum of all Proximity Values
Δ_{max}	Maximum of all Proximity Values
ρ	Distinguishing Coefficient
n	Total Number of Working Conditions

References

1. Ai, X.M.; Yi, J.Y.; Zhao, H.; Chen, S.Q.; Luan, H.; Zhang, L.D.; Feng, D.C. An empirical predictive model for the dynamic resilient modulus based on the static resilient modulus and California bearing ratio of cement- and lime-stabilised subgrade soils. *Road Mater. Pavement Des.* **2021**, *22*, 2818–2837. [CrossRef]
2. Zhang, J.H.; Peng, J.H.; Zeng, L.; Li, J.; Li, F. Rapid estimation of resilient modulus of subgrade soils using performance-related soil properties. *Int. J. Pavement Eng.* **2021**, *22*, 732–739. [CrossRef]
3. Yang, X.J.; Wang, J.M.; Hou, D.G.; Zhu, C.; He, M.C. Effect of dry-wet cycling on the mechanical properties of rocks: A laboratory-scale experimental study. *Processes* **2018**, *6*, 199. [CrossRef]
4. Shi, G.M.; Li, X.Y.; Guo, Z.K.; Zhang, Z.Z.; Zhang, Y.Y. Effect of mica content on shear strength of the Yili loess under the dry-wet cycling condition. *Sustainability* **2022**, *14*, 9569. [CrossRef]
5. Bai, Y.; Ye, W.J.; Wu, Y.T.; Chen, Y.Q. Multiscale analysis of the strength deterioration of loess under the action of drying and wetting cycles. *Adv. Mater. Sci. Eng.* **2021**, *2021*, 6654815. [CrossRef]
6. Zheng, J.L.; Zhang, R.; Yang, H.P. Highway subgrade construction in expansive soil areas. *J. Mater. Civ. Eng.* **2009**, *21*, 154–162. [CrossRef]
7. Zhang, R.; Liu, Z.N.; Zheng, J.L.; Lei, G. Utilisation of expansive soils as highway embankment materials in humid environments. *Int. J. Pavement Eng.* **2022**, *23*, 2176–2190. [CrossRef]
8. Yuan, J.B.; He, Y.; Liu, J.H. Construction of weak expansive red clay on dongxin expressway in Hunan Province, China. *J. Perform. Constr. Facil.* **2016**, *30*, C4015001. [CrossRef]

9. Puppala, A.J. Performance evaluation of infrastructure on problematic expansive soils: Characterization challenges, innovative stabilization designs, and monitoring methods. *J. Geotech. Geoenviron. Eng.* **2021**, *147*, 04021053. [CrossRef]
10. Snethen, D.R.; Townsend, F.C.; Johnson, L.D.; Patrick, D.M.; Vedros, P.J. *A Review of Engineering Experiences with Expansive Soils in Highway Subgrades*; Federal Highway Administration, Offices of Research and Development: Washington, DC, USA, 1975.
11. Murali, K.; Ashok, S.; Giridharan, N.; Pandiarasan, K.; Logesh, P. A review on stabilization of expansive soil with various admixtures. *Int. J. Sci. Res. Publ.* **2018**, *8*, 7629. [CrossRef]
12. Gaikwad, M.V.; Singh, S.K.; Suryavanshi, N.T.; Survase, K.P.; Yadav, S.R.; Pujari, M.C.; Basate, O.S. Reviewing the enhancement of expansive soil through different waste material blending. *World J. Adv. Eng. Technol. Sci.* **2024**, *11*, 158–166. [CrossRef]
13. Sambre, T.; Endait, M.; Patil, S. Sustainable soil stabilization of expansive soil subgrades through lime-fly ash admixture. *Discov. Civ. Eng.* **2024**, *1*, 65. [CrossRef]
14. Yu, D.F.; Duan, H.B.; Song, Q.B.; Li, X.Y.; Zhang, H.; Zhang, H.; Liu, Y.C.; Shen, W.J.; Wang, J.B. Characterizing the environmental impact of metals in construction and demolition waste. *Environ. Sci. Pollut. Res.* **2018**, *25*, 13823–13832. [CrossRef] [PubMed]
15. Lauritzen, E.K. *Construction, Demolition and Disaster Waste Management: An Integrated and Sustainable Approach*; CRC Press: Boca Raton, FL, USA, 2018.
16. Duan, X.; Wang, Y.; Yang, D.; Zeng, W.; Du, Y.; Li, N. Evaluation of road performance and carbon emission accounting analysis of recycled aggregates from construction and demolition waste. *Sci. Rep.* **2025**, *15*, 29395. [CrossRef]
17. Paula Junior, A.C.; Jacinto, C.; Turco, C.; Fernandes, J.; Teixeira, E.; Mateus, R. Analysis of the effect of incorporating construction and demolition waste on the environmental and mechanical performance of earth-based mixtures. *Constr. Build. Mater.* **2022**, *330*, 127244. [CrossRef]
18. Cabalar, A.; Zardikawi, O.; Abdulnafaa, M. Utilisation of construction and demolition materials with clay for road pavement subgrade. *Road Mater. Pavement Des.* **2019**, *20*, 702–714. [CrossRef]
19. Kianimehr, M.; Shourijeh, P.T.; Binesh, S.M.; Mohammadinia, A.; Arulrajah, A. Utilization of recycled concrete aggregates for light-stabilization of clay soils. *Constr. Build. Mater.* **2019**, *227*, 116792. [CrossRef]
20. Islam, S.; Islam, J.; Hoque, N.M.R. Improvement of consolidation properties of clay soil using fine-grained construction and demolition waste. *Heliyon* **2022**, *8*, e11029. [CrossRef] [PubMed]
21. Zaharieva, R.; Evlogiev, D.; Kerenchev, N.; Stanimirova, T. Modification of quaternary clays using recycled fines from construction and demolition waste. *Processes* **2022**, *10*, 1062. [CrossRef]
22. Liu, C.H.; Hung, C. Reutilization of solid wastes to improve the hydromechanical and mechanical behaviors of soils—A state-of-the-art review. *Sustain. Environ. Res.* **2023**, *33*, 17. [CrossRef]
23. *JTG 3430-2020*; Test Methods of Soils for Highway Engineering. Ministry of Transport of the People's Republic of China: Beijing, China, 2020.
24. *JTG/T 3610-2019*; Technical Specifications for Construction of Highway Subgrades. Ministry of Transport of the People's Republic of China: Beijing, China, 2019.
25. Ahmadi, M.; Shire, T.; Mehdizadeh, A.; Disfani, M. DEM modelling to assess internal stability of gap-graded assemblies of spherical particles under various relative densities, fine contents and gap ratios. *Comput. Geotech.* **2020**, *126*, 103710. [CrossRef]
26. Zhang, F.S.; Li, M.L.; Peng, M.; Chen, C.; Zhang, L.M. Three-dimensional DEM modeling of the stress-strain behavior for the gap-graded soils subjected to internal erosion. *Acta Geotech.* **2019**, *14*, 487–503. [CrossRef]
27. Niu, Z.L.; Xu, J.; Li, Y.F.; Wang, Z.F.; Wang, B. Strength deterioration mechanism of bentonite modified loess after wetting-drying cycles. *Sci. Rep.* **2022**, *12*, 3130. [CrossRef]
28. Hao, R.H.; Zhang, Z.Z.; Guo, Z.Z.; Huang, X.B.; Lv, Q.L.; Wang, J.H.; Liu, T.C. Investigation of changes to triaxial shear strength parameters and microstructure of Yili loess with drying-wetting cycles. *Materials* **2022**, *15*, 255. [CrossRef]
29. Zhao, Y.B.; Yang, C.Q.; Qu, F.; Wu, Z.R.; Ding, K.J.; Liang, Z.S. Effect of wet-dry cycles on the mechanical performances and microstructure of pisha sandstone. *Molecules* **2023**, *28*, 2533. [CrossRef] [PubMed]
30. Gu, C.; Gu, Z.Q.; Cai, Y.Q.; Wang, J.; Ling, D.S. Dynamic modulus characteristics of saturated clays under variable confining pressure. *Can. Geotech. J.* **2017**, *54*, 729–735. [CrossRef]
31. Chu, C.F.; Zhan, M.H.; Feng, Q.; Li, D.; Xu, L.; Zha, F.S.; Deng, Y.F. Effect of drying-wetting cycles on engineering properties of expansive soils modified by industrial wastes. *Adv. Mater. Sci. Eng.* **2020**, *2020*, 5602163. [CrossRef]
32. Wang, R.; Hu, Z.P.; Ren, X.; Li, F.T.; Zhang, F. Dynamic modulus and damping ratio of compacted loess under long-term traffic loading. *Road Mater. Pavement Des.* **2022**, *23*, 1731–1745. [CrossRef]
33. Zhang, F.Z.; Chen, X.P. Influence of repeated drying and wetting cycles on mechanical behaviors of unsaturated soil. *Chin. J. Geotech. Eng.* **2010**, *32*, 41–46.
34. Tang, C.S.; Bin, S.; Chun, L. Study on desiccation cracking behaviour of expansive soil. *J. Eng. Geol.* **2012**, *20*, 663–673.
35. Singer, M.; Southard, R.; Warrington, D.; Janitzky, P. Stability of synthetic sand-clay aggregates after wetting and drying cycles. *Soil Sci. Soc. Am. J.* **1992**, *56*, 1843–1848. [CrossRef]

36. An, R.; Kong, L.W.; Zhang, X.W.; Li, C.S. Effects of dry-wet cycles on three-dimensional pore structure and permeability characteristics of granite residual soil using X-ray micro computed tomography. *J. Rock Mech. Geotech. Eng.* **2022**, *14*, 851–860. [CrossRef]
37. Zhao, Y.; Zhang, H.R.; Wang, G.Y.; Yang, Y.Q.; Ouyang, M. Development characteristics and mechanism of crack in expansive soil under wet-dry cycling. *Appl. Sci.* **2024**, *14*, 6499. [CrossRef]
38. Zhou, W.; Cheng, J.L.; Zhang, G.K.; Li, H.B.; Cheng, Y.G.; Ma, G.; Ji, X. Effects of wetting-drying cycles on the breakage characteristics of slate rock grains. *Rock Mech. Rock Eng.* **2021**, *54*, 6323–6337. [CrossRef]
39. Wu, H.; Shao, S.; Shao, S.J.; Zhang, S.Y.; Wang, Z.C. Variations in dynamic shear modulus of loess exposed to dry-wet cycles from Xi'an area, China. *Soil Dyn. Earthq. Eng.* **2023**, *173*, 108126. [CrossRef]
40. Abbey, S.J.; Amakye, S.Y.O.; Eyo, E.U.; Booth, C.A.; Jeremiah, J.J. Wet-Dry Cycles and Microstructural Characteristics of Expansive Subgrade Treated with Sustainable Cementitious Waste Materials. *Materials* **2023**, *16*, 3124. [CrossRef]
41. Zhang, J.H.; Zhang, A.S.; Li, J.; Li, F.; Peng, J.H. Gray correlation analysis and prediction on permanent deformation of subgrade filled with construction and demolition materials. *Materials* **2019**, *12*, 3035. [CrossRef]